SailMAV: design and implementation of a novel multi-modal flying sailing robot

Raphael Zufferey, Alejandro Ortega Ancel, Célia Raposo, Sophie F. Armanini, André Farinha, Robert Siddall, Ion Berasaluce, Haijun Zhu and Mirko Kovac

***Abstract*— Despite significant research progress on small-scale aerial-aquatic robots, most existing prototypes are still constrained by short operation times and limited performance in different fluids. The main challenge is to design a vehicle that satisfies the partially conflicting design requirements for aerial and aquatic operation. In this paper we present a new class of aerial-aquatic robot, the Sailing Micro Air Vehicle, 'SailMAV'. Thanks to a three-part folding wing design, the SailMAV is capable of both flying and sailing. The robot design permits long and targeted missions at the water interface by leveraging the wind as movement vector. It simultaneously offers the flexibility of flight for rapidly reaching a designated area, overcoming obstacles and moving from one body of water to another, which can be very useful for water sampling in areas with many obstacles. With a total wingspan of 0.96 m, the SailMAV employs the same wing and actuation surfaces for sailing as for flying. It is capable of water surface locomotion as well as take-off and flight at a cruising speed of 10.8 ms^{-1}. The main contributions of this paper are (i) new solutions to the challenges of combined aerial and aquatic locomotion, (ii) the design of a novel hybrid concept, (iii) the development of the required control laws, and (iv) the demonstration of the vehicle successfully sailing and taking off from the water. The presented work can inform the design of hybrid vehicles that adapt their morphology to move effectively.**

I. Introduction

Inspired by nature, multi-modal robots are defined by their ability to move efficiently in different media (i.e. water, air and/or ground) and transition repeatedly between these. Thanks to this unique capability, multi-modal robots can combine the most advantageous features of different types of robots, e.g. the rapid deployment of fixed-wing air vehicles and the long-duration mission capability of water surface vehicles. Hence, while such robots are challenging to develop, due to the considerably different conditions entailed by different media, they would allow for significant improvements in many important applications. A notable example is water sampling: an essential activity for purposes such as scientific measurements, pollution and environmental monitoring, or underwater surveying. At present water sampling either relies on slow, complex, often human-controlled integration of different types of vehicles, [1], [2], or is constrained by the use of a single type of vehicle.

Manuscript received: February 25, 2019; revised: May 21, 2019. This paper was recommended for publication by Editor Jonathan Roberts upon evaluation of the Associate Editor and Reviewers comments. This work was funded by EPSRC (EP/R009953/1) and the Royal Society Wolfson fellowship (RSWF/R1/18000).

All the authors are with the Aerial Robotics Laboratory, Imperial College London, UK, r.zufferey16@imperial.ac.uk.

Digital Object Identifier (DOI): see top of this page.

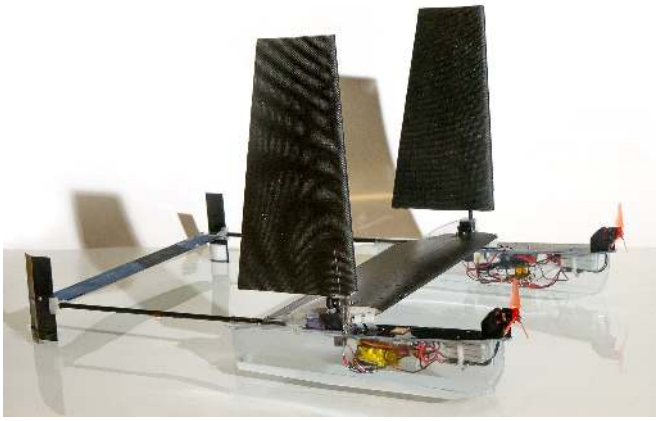

Fig. 1. SailMAV side view

As a first step towards autonomous water sampling, several autonomous underwater vehicles and autonomous water surface vehicles (AUVs and ASVs) have been developed for such applications (e.g. [3], [4], [5], [6]), however these vehicles are inherently limited to specific operating conditions. The Saildrone [7], for instance, is currently autonomously roaming the ocean for marine investigation, for applications such as animal tracking and environmental monitoring. At 750 kg, however, this robot, like most AUVs, is constrained to large bodies of water and long-duration missions, while it would be ill-suited for small bodies of water, shallow waters or shorter missions where fast results are critical.

Clearly, the ability to transition to flight would vastly extend the potential and capabilities of AUVs and ASVs, allowing for extremely fast deployment, rapid coverage of extensive distances, overflying of obstacles and autonomous transition between different bodies of water. In addition, the possibility of landing on the ground would eliminate the need for a boat or port to recover the robot. Flight capability would also allow for aerial photography, providing information that cannot be obtained solely from the shore or water surface.

Recently, a number of quadrotors have achieved aquatic take-off [8], [9]. The Looncopter [8], for example, shows underwater locomotion with the same propellers as for flight, as well as water-air transitioning, making it applicable for short, fast and flexible missions. This aircraft is however subject to the short lifetime and range of multirotors. Fixed-wing designs [10], [11], [12] improve on the aforementioned limitations, but typically do not show mobility on the water

surface or underwater. The AquaMAV vehicle [13], [14] demonstrates rapid water escape, with a flying range of 5 km, achievable thanks to the fixed-wing configuration. Underwater operation is rendered possible through a dual-speed propeller [15], and take-off through the release of high-pressured CO_2. However, a full mission cycle has not yet been demonstrated, and prolonged mobile water sampling is a challenge also for this robot.

As evident from the above discussion, despite the recent advances in small aerial-aquatic robots [16], [1], no existing device of this type can sustain long-duration missions. In this paper, we propose a new device class that can perform aquatic investigation whilst offering the flexibility of flying. The SailMAV exhibits multiple take-offs, transition to flight as well as passive water surface locomotion. Moreover, it leverages environmental vectors, i.e. wind to propel itself through the water and solar energy to recharge its batteries for the next flight. In this way, long-duration missions become possible with only minimal energy expenditure, while at the same time the benefits of aerial locomotion can be fully exploited.

II. Multi-modal locomotion concept

An aerial-aquatic robot poses substantial opposing constraints. Its weight needs to be minimized for take-off yet the aquatic environment requires adequate waterproofing as well as bulky buoyancy elements that negatively affect flight. Furthermore, a research robot should be highly modular for adjustments and continuous upgrades, which also increases its weight. This article discusses how to balance these elements effectively to obtain a 520 g field-ready autonomous hybrid vehicle.

A key requirement in the development of a lightweight hybrid aircraft is the reduction of complexity. We tackle this task by employing the same control surfaces for flying as for sailing. Despite the three order of magnitude difference in density of air and water, we use the same actuators and electronic configuration for both air and water mobility.

The proposed robot concept features a three-segment wing, i.e. a *central wing* terminated on its extremities by two variable-pitch wings. The latter two surfaces pivot upwards during sailing and will be referred to as *sails* for clarity, even in flight mode.

The SailMAV is designed to execute a repeated sail-fly-sail cycle. It *sails* on the surface of the water, propelled by the wind, whilst fulfilling its scientific mission and recharging its small battery. During water locomotion, an autonomous sailing controller ensures that the robot can move to specific waypoints. When a change of body of water is required, a large distance needs to be covered or an obstacle obstructs its way, the vehicle switches to *flight* mode. The take-off and flying phases use a standard fixed-wing flight controller. The batteries with a capacity of 600 mAh are sufficient for a 7 km flight, at 10.8 ms^{-1} cruise speed. Finally, the vehicle lands on water again for its next sensing mission.

The transition to flight is composed of three phases, as described in the seaplane literature [17] and shown in Fig. 2. First, the propellers are turned on and the robot is in a low-speed regime, i.e. the hulls are in the water and the plane behaves as a displacement vessel. As the speed increases, the robot moves to a planing range (phase 2), passing the point of highest water resistance called the hump. When planing, it touches the water only at the afterbody section of the boat. Planing is assisted by the central wing, which increases the lift substantially through *ground effect*, providing up to 28% additional lift, see section IV. Thirdly, full flight is achieved after take-off and the aircraft behaves as a standard fixed-wing vehicle.

III. Design and system

A. Structure

The SailMAV is composed of a carbon fibre, foam and shells structure (Fig. 3). A lead design driver of this structure is its repairability. As the robot is a research platform, each of its component should be replaceable. We therefore opted for a top plate closure of the two hulls, allowing full access to the electronics. The robot features two vacuum-formed symmetrical hulls for flotation (0.5 mm PVC), as well as electronics and motor mounts.

The hulls are linked by a rigid closed-cell wing, with a high-performance polymethacrylimide (PMI) foam core, sandwiched around a data and power bus. The wings are wrapped with one layer of ultrathin 100 μm woven dry carbon fibre fabric via a wet-layup process. Epoxy resin is poured onto the fabric and applied around the foam cores, and the resulting composite is cured at 65°for 7 hours between two compressed female molds. This method provides outstanding strength and resilience to crushing with a short manufacturing cycle of approximately one day. The central wing weighs 52 g. At the end of each hull two carbon-fibre tubes are affixed, which compose the tail and carry the drive wires (0.6 mm steel) for the control surfaces.

B. Actuation

One of the key challenges is to develop a mechanism allowing the morphology of the sails to change. A key requirement to this actuator is non-reversibility without being powered, as both modes will be enabled for prolonged periods. Our custom actuator shown in Fig. 4 features a rotating stainless steel, laser-sintered *cam*. This pivoting part is locked from rotating in both directions when it sits at an extremity. A small double switch and controller ensures that the lead screw moves the cam from one position to the other. This folding mechanism only draws current when rotating the cam. The whole actuator is covered by an airfoil-shaped shell for fixation and water-tightness.

As shown in Fig. 4, by rotating around the longitudinal body axis, the sails can assume two different orientations: 90° for sailing, i.e. exactly vertical, and 6° for flight. The dihedral angle is chosen at 6°to improve roll stability in flight configuration and can be changed at will by replacing the cam. Moreover, in both modes, each sail can rotate around itself, thanks to a built-in servo, to control the plane in roll (flight) and to orient the sails (sailing).

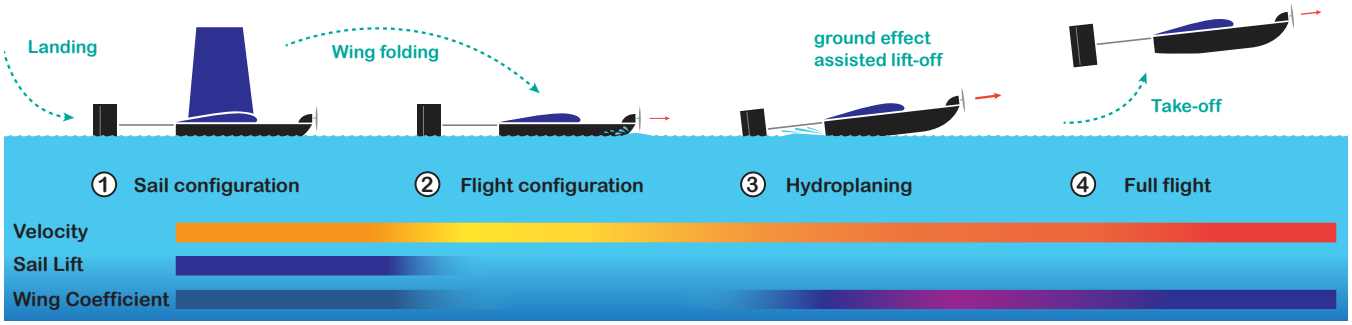

Fig. 2. Sailing-flight cycle overview. The robot lands on water where it transitions to a *sailing* configuration and executes its mission. Take-off is achieved via propelled acceleration, transitioning from displacement vessel regime, to hydroplaning and lastly to being fully airborne

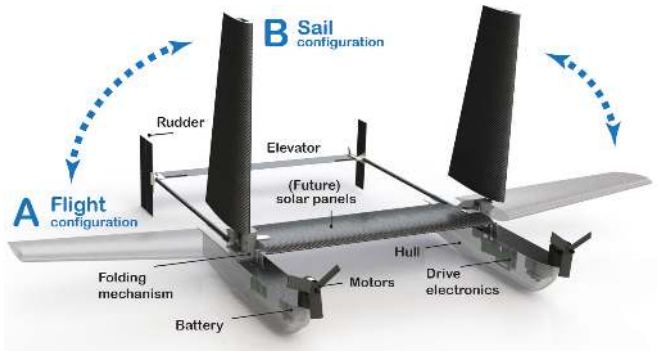

Fig. 3. Schematic clarifying the two modes of operation of the robot. A. The sail in flying configuration, showing a 6°angle to the horizontal. B. The sail is moved to an upright position, for the sailing configuration

The tail is actuated by two servos, located in each hull. One moves the elevator for pitch control, while the second actuates the rudder. The rudder controls the robot's yaw orientation both in flight and in sailing.

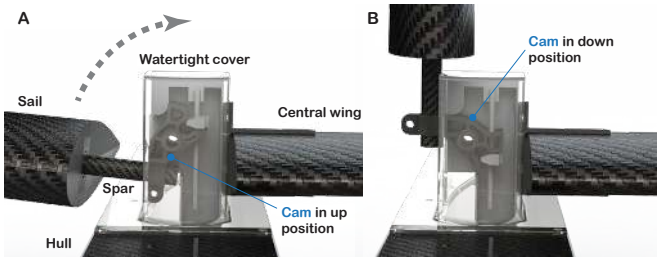

Fig. 4. A. The sail in flying configuration, showing a 6° angle to the horizontal. B. The sail is moved to the upright position, for sailing. This mechanism is double locking, the central cam is irreversible at both ends of the lead screw.

C. Avionics

The robot is controlled by a Pixracer flight microcontroller running the *px4* firmware. Featuring an ARM M4 running at 180 MHz, it outputs the signals to the 8 actuators and reads all onboard sensors. It is connected in the left hull to a power and signal PCB custom-designed for the robot. This board is the interface with the *central wing bus* (CWB), a 16-line link to the right hull. In addition, the folding actuator as well as the tail and sail servo are also connected to the board.

Two batteries resting in each hull are connected in parallel for mass symmetry feeding 16 V voltage to the ESCs and the voltage regulator which powers both the controller and the actuators independently. Both the 16 V and regulated 5 V lines are distributed on both hulls via the CWB.

Three sensors are located onboard, sending live data for measurement and control. A GPS receiver with barometer ensures stable flight in outdoor tests as well as room for expansion towards waypoint-based control. When navigation data is unavailable, e.g. when moving indoors, wind velocity is obtained from a pitot tube air speed sensor. To the best of our knowledge, no such lightweight wind angle sensor exists. The sensors are distributed between the hulls to achieve a balanced aircraft.

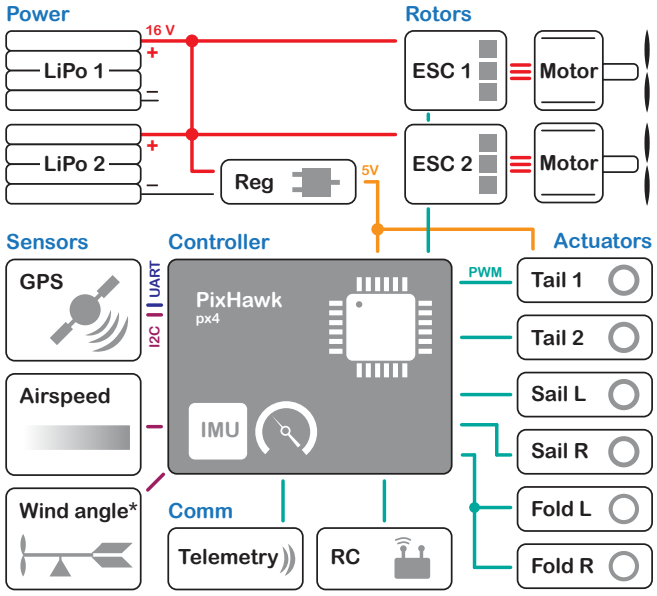

Fig. 5. Overview of the electronic layout of the proposed concept. A central PixHawk, located in the right hull communicates with 3 sensors for controllability, 2 communication links and 8 actuators in total, spread between the two hulls. The device is powered by four cell 300 mAh lithium polymer batteries, one in each hull. The wind angle sensor (*) is in development

D. Hull design

The design of the hulls has a direct impact on the performance in sailing and take-off.

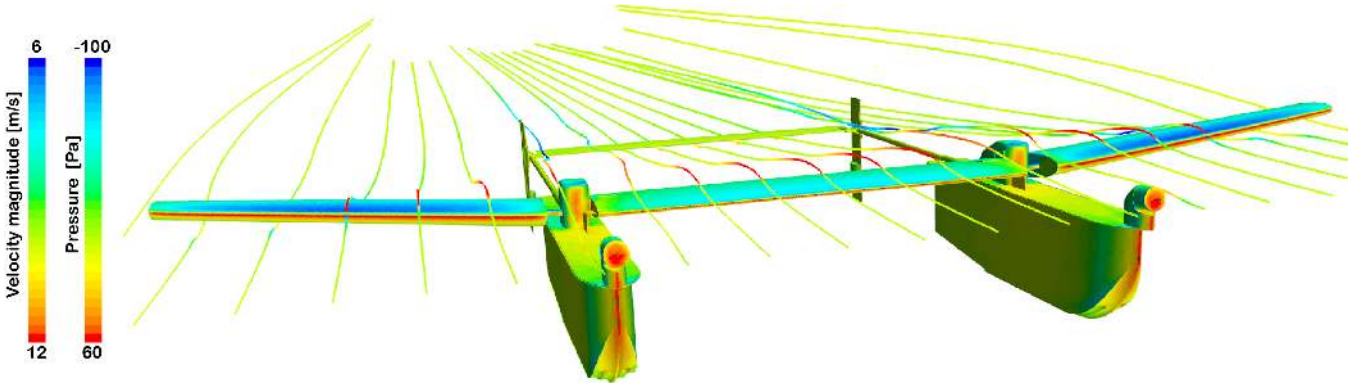

Fig. 6. Static pressure contours on the surface of SailMAV, with streamlines colored by velocity magnitude for a free-stream velocity of 10 ms^{-1} and central wing angle of attack of 5.75°.

During sailing, the robot is in displacement regime, during which the entire weight of the robot is supported by its buoyancy. This creates drag not only in forward motion, but also in the lateral direction. Whilst the former is disadvantageous during sailing and take-off, the latter is beneficial for sailing as it opposes drifting in cross-wind. In order to take advantage of this during sailing but still achieve an efficient take-off, it is essential to design the hulls with a high length to beam ratio, the beam being the width of the hull.

In hydroplaning, the velocity of the craft is sufficient for the hydrodynamic lift forces to enable positive trim angles and the emergence of the bow and the majority of the hull from the waterline. A parameter that influences the transition to this regime is the location and size of the step separating the forebody and afterbody of the hull. This step is ideally placed at the location where the coefficient of pressure is lowest, however this measurement requires complex experiments or detailed simulations with previous knowledge of the hull shape. In this pilot design, the guidelines in [18] were followed and thus the step was placed 10°aft of the centre of gravity to allow the aircraft to rotate easily during take-off. The hull was then designed with a length to beam ratio of 11 with a step located at two thirds of the hull length, an afterbody angle of 7°which limits the planing trim angle (ensuring the tail does not pierce the water interface during planing), and a set of chines that drive the spray away from the propellers. The width of the hull was left as an adjustable parameter and a simple theoretical study performed to predict the transition to planing. The important non-dimensional parameters were identified as the beam loading coefficient, the Froude number and the lift coefficient:

$$C_\Delta = \frac{\Delta_0}{\rho_{H_2O} b^3}, \quad C_U = \frac{U}{\sqrt{gb}}, \quad C_L \sim \frac{C_\Delta}{{C_U}^2} \tag{1}$$

Where Δ_0 corresponds to the ship's displacement or mass and b is the beam length. The characteristic length was taken as b for these numbers, in accordance with [19] and [20]. From the analysis performed in the latter reference, an empirical expression for the lift of planing hulls was obtained:

$$C_L = \tau^{1.1} \left(0.0120\gamma^{1/2} + \frac{0.0055\gamma^{5/2}}{{C_V}^2} \right) \tag{2}$$

Where τ is the trim angle estimated as the afterbody angle, and γ the wetted hull length given by $\gamma = \gamma_l + 0.3$. Even though within the C_U, τ and γ bounds of applicability imposed by the author, these expressions have not been demonstrated for hulls of this scale, thus more research is needed in this area. Using both definitions of C_L, where the contribution of buoyancy is considered negligible and thus $L = \Delta_0 g$, one can find an asymptotic relation between the beam width and the planing velocity. By selecting beam length values matching the C_Δ of seaplane hulls in Ref. [17], a hull geometry was finally selected.

IV. Aerodynamics

An effective aerodynamic design is critical to the success of the robot's mission. Its objectives are to provide sufficient lift for take-off and cruise and to minimise drag, in order to achieve a long range and endurance, while maintaining adequate flight stability and manoeuvrability. The first step was choosing airfoils for the central wing and wing-sails. We chose the S6061-il cambered airfoil for the central wing due to its high lift-to-drag ratio of 51.2 and good stall characteristics at the flight Reynolds number range of 80,000 to 120,000. The wing-sails, however, were designed to be symmetrical to ensure symmetrical wind loading during sailing. Consequently, we chose the S8035 airfoil due to its efficiency and high stall angle at low Reynolds numbers as well as its large thickness, which allows enough space to house the servo. The central wing was chosen to be rectangular, while the wing-sails have a taper ratio of 0.6. The sails are tapered towards the tip in order to reduce induced drag, structural loads at the root as well as loads on the servos. The central wing was installed at an angle of 5.75° to the hulls, which corresponds to the maximum lift-to-drag angle of attack for the chosen airfoil. The angle of attack of the wing-sails, however, is variable and can be controlled by the servo. The default angle of attack for the wing-sails was chosen to be 7.75°, since their airfoil stalls at a 2° higher angle than that of the central wing, allowing maximum lift for both the central wing and wing-sails at the same time, thus maximising take-off performance and minimising stall speed.

The empennage was designed to work effectively in both air and water. We chose an H-tail configuration, with the

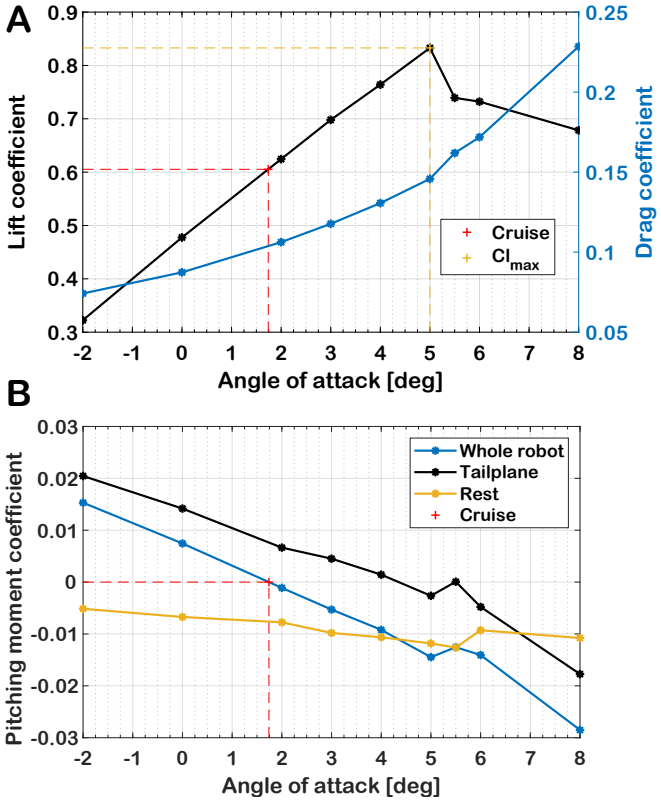

Fig. 7. A. Lift (black) and drag (blue) coefficient variation with angle of attack, showing the cruise condition at 1.8° and stall at 5°. B. Pitching moment coefficient about the center of gravity for the whole robot, tailplane, and robot minus tailplane. The plot shows that the SailMAV is trimmed at the cruise condition and that it is longitudinally stable, presenting a negative slope for pitching moment, except immediately after stall.

tailplane in between the fins for structural rigidity. Both the tailplane and the fins consist of a carbon fibre plate with half-round carbon fibre stiffeners for light weight and ease of manufacture. The fins and rudder extend downward from the tailplane, as well as upward, so that enough fin and rudder area are underwater, ensuring sufficient control during sailing and take-off. The tailplane and fin volume coefficients are 0.47 and 0.04 respectively.

A. Numerical simulation setup

A computational fluid dynamics study (CFD) was conducted in order to verify the aerodynamic design choices, to assist in tuning the flight controls and to determine flight performance. The simulation setup, calculation of the solution and post-processing were carried out with STAR-CCM+ 12.06.010-R8. The computational domain consists of an elliptical cross-section with semi-minor and semi-major axes of 0.96 m and 1.44 m and respectively, extruded 4 m in the flow direction, 1 m upstream and 2.38 m downstream of the robot. A mesh study was conducted, for which the size of the cells was reduced until the results converged. The final mesh chosen consisted of 3,748,686 mesh cells, formed mostly of polyhedral cells, with 8 layers of prism cells on the wall surfaces. We modelled turbulence using K-Omega SST, with gamma transition prediction. We completed simulations at angles of attack for the hulls from -2° to 8°, corresponding to central wing angles of 3.75° to 13.75°, with higher angle resolution near stall. All simulations were done at a Reynolds number of 96,000 based on the central wing chord, which corresponds to a flight speed of 10 ms^{-1} at standard atmospheric conditions.

In order to determine the robot's performance and longitudinal stability during take-off and landing, simulations were also done taking the surface of the water into account. The physics parameters are the same as for the free-stream simulations, but the domain is cut at the bottom to create another boundary at the water surface. Simulations were performed with the robot at its point of maximum submersion, as well as at its hydroplaning position on the verge of take-off.

B. Numerical simulation results

Fig. 7A shows the lift coefficient (C_l) and drag coefficient (C_d) as a function of the angle of the SailMAV's hull and tail assembly. We show that the lift increases up to an angle of attack of 5°, when the robot stalls. At this point, the C_l is 0.833, which corresponds to a stall speed of 9.3 ms^{-1}. The lift coefficient at the cruise condition is shown to be 0.605, which yields a cruise speed of 10.8 ms^{-1}. Using the C_d of 0.102 for the cruise condition, the drag, and therefore required thrust, for cruise are calculated to be 0.86 N.

Fig. 7B shows how the pitching moment coefficient about the centre of mass changes with the angle of attack. The SailMAV is shown to be trimmed, requiring no elevator deflection at the cruise angle of attack of 1.8°. The pitching moment slope with angle of attack is shown to be negative, except immediately after stalling, resulting in the robot being longitudinally stable in flight.

The simulations in ground effect show that the lift coefficient when closest to the water surface, with the central wing being 88 mm from the water, is 28% higher than when out of ground effect, while the drag coefficient is 1% lower. This higher lift generated as the robot accelerates enables it to escape the large hydrodynamic drag from the submerged hulls. As SailMAV transitions to hydroplaning, the robot raises a further 34 mm above the water, resulting in lift and drag coefficients of 23% and 2% higher than for the cruise condition. This results in a take-off speed 5% lower that without ground effect.

V. Control and Autonomy

The robot needs radically different control plans for the flying phase and the sailing phase. Fig. 8 shows the core control elements required for our hybrid design. The flight controller leverages existing standard fixed-wing airframe controllers. In this mode, standard controls are available, namely elevator, rudder and propellers. In addition, the two sails act as independently actuated flaps. The fixed-wing controller is available within the open-source control framework *px4* [21]. Based on PID control laws, a dedicated module dictates how roll, pitch and yaw inputs translate into actuator commands. Take-off and landing are also handled by the standardized software. An Extended Kalman Filter (EKF) runs on a separate thread and publishes the estimated

attitude and position based on the sensor data, i.e. GPS, double IMU, barometer and air speed sensor. Note that not all measurements obtained by the robot (and shown in Fig. 8 are necessary for the current controller.

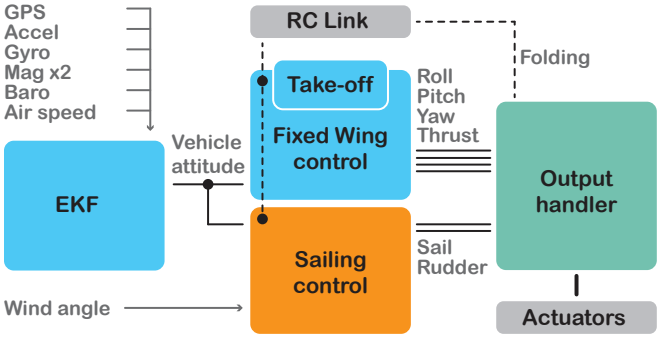

Fig. 8. Control diagram of the hybrid controller. The pre-existing modules from the *px4* framework are blended with a new sailing control module and an adapted output handler that serves correct values to the actuators.

Once the robot has landed on the water, the sailing controller is enabled via telemetry instructions. The custom module follows the px4 framework and is compiled as part of the software. It listens to the *vehicle attitude* estimated by the EKF and extracts the yaw angle (with respect to the magnetic north, according to a north-east-down coordinate frame). We will rely on a new wind sensor that measures the *wind angle* relative to the robot (Ψ_{WB}). Based on the aforementioned data, the following control law was implemented to calculate the *sail angle*.

$$\delta_{sail} = -\frac{\pi}{4}\text{sgn}\left(\Psi_{WB}\right)\left(\cos\Psi_{WB}+1\right) \tag{3}$$

where Ψ_{WB} is the angle of the boat relative to the wind and is defined by the following relation, bounded by $\pm\pi$:

$$\Psi_{WB} = \left[\left(\Psi_W - \Psi_B + \pi\right) \bmod \left(2\pi\right)\right] - \pi \tag{4}$$

Note that if a wind sensor is available, the angle Ψ_{WB} can be obtained directly, as long as it is wrapped to the interval $[-\pi, \pi]$. Eq. 3 yields the sail angle with respect to the boat, and is a modification of the expression presented in Refs. [22], [23]). This formulation ensures that the sail flips from one side of the boat to the other when pointing downwind, while in the upwind boat orientation, the function goes through a continuous zero, as wanted. If sufficient actuation range is available, the sail is perpendicular to the wind when moving downwind. If a 90° angle is not achievable, as in the current vehicle, the actuators will saturate and remain at their maximum opening angle once reached (cf. Fig. 11 in Sec. VI).

Given that the current wind sensor cannot measure the wind speed, the sail control law was based only on the relative orientation of boat and wind. A more advanced formulation will be developed which will take the apparent wind speed into account. While the current sailing control scheme is basic, it allows for autonomous sail orientation, thus enabling the boat to exploit the available wind as best possible, and highlighting one of the key capabilities of the developed robot. Note that the sail is adjusted exclusively to fulfil this purpose, while the heading is adjusted using the rudder.

Future work will extend the functionalities of the sail controller to include autonomous path-following, as well as additional modes to permit the boat to move upwind with a tacking strategy, to turn downwind without losing speed via a gybing manoeuvre, and to move in the absence of wind, exploiting the propellers.

VI. Results

A. Mass budget

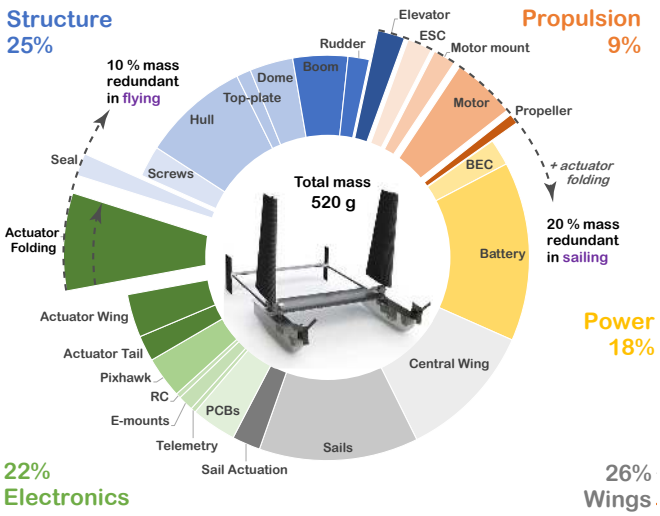

Fig. 9. Mass distribution of SailMAV, split into five categories: structure, propulsion, electronics, power and wings. The exploded bars show the *penalty* associated with the hybrid design in both sailing and flying

One of the fundamental issues with hybrid designs is the mass penalty in each of the different modes. The developed robot has 10% redundant mass in flight, linked to the waterproofing and the folding of the wings, both of which are unnecessary in flight. In sailing, the entire propulsion block, including motor and drivers is redundant. The folding of the wing element is also irrelevant, bringing the penalty during sailing to 20%. This extra weight will lower the water line and have a minor impact on the sailing performance.

The SailMAV carries a total of 22% in mass of electronics, which comprises all the elements required for manual as well as fully autonomous flight and actuation in all modes. In addition, a quarter of the weight is needed for electrically powering the robot and propulsion. Battery weight is minimal, representing 14% of the total weight, as the batteries are only required for take-offs and short flights. The last 50% of the robot mass is structure and wings, making both flight and sailing possible. The ultralight composite wings could be extended with minor weight penalty, lowering minimum flight speeds further.

B. Transition from water to flight

Hydroplaning was tested in a shallow water tank (10 cm depth), in calm, controlled conditions, and was achieved within 5 m, at full throttle with a wide hull shape. Fig. 12(a)

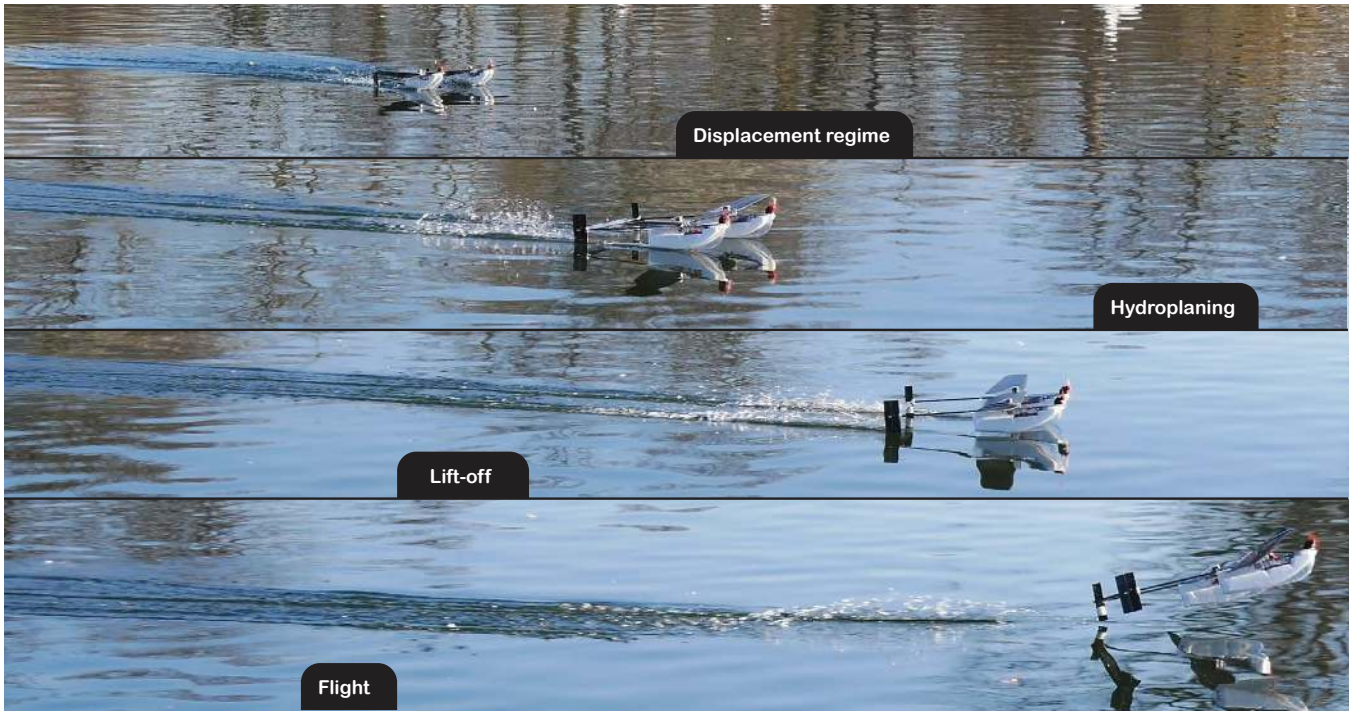

Fig. 10. Flight-sailing-flight cycle overview. The robot lands on water where is transitions to a *sailing* configuration and executes its mission. Take-off is achieved via propelled acceleration, transitioning from displacement vessel regime, to hydroplaning and lastly to being fully airborne

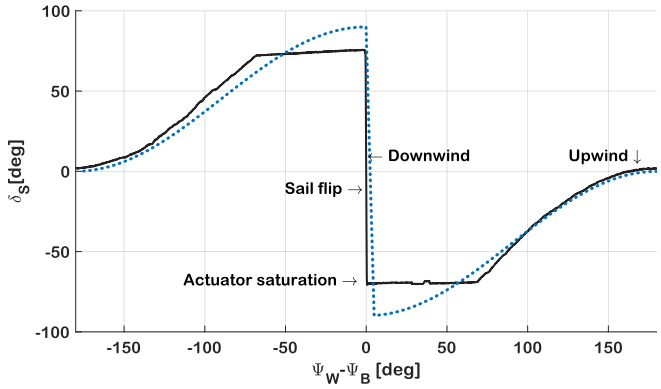

Fig. 11. Sail angle controller (doted line) with respect to relative wind orientation (i.e. wind-to-body angle). The solid line shows how the sail behaves experimentally: here, saturation occurs at around 65°, due to the limited servo range.

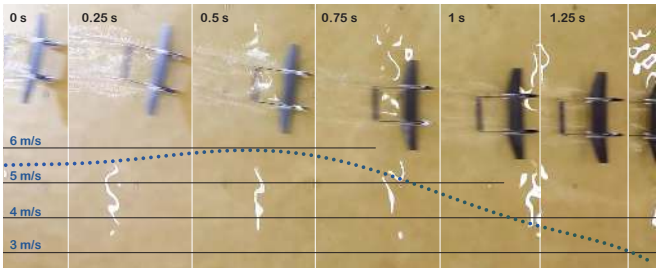

(a) Hydroplaning

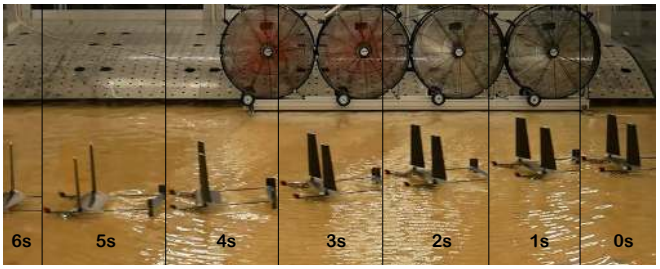

(b) Sailing

Fig. 12. Test results showing examples of the hydroplaning phase immediately prior to take-off, and of the sailing phase.

shows a top view of the final part of the trajectory in one of these tests, where a maximum velocity of $6\,\mathrm{ms}^{-1}$ was achieved, slightly below take-off speed.

Outdoor experiments were also performed to assess the robot's transition from water to flight, as for example shown in Fig. 10, which presents the different phases of the transition. In the displacement regime, the robot is moving slowly and the hulls are fully in the water. It can also be seen that the tail is submerged during the moments before transition to hydroplaning, which creates spray and considerable drag. This is however not the case at lower speeds or during hydroplaning. Increasing the beam of the hulls was found to help reducing the spray towards the propulsion system, which prevented the robot from accelerating effectively for lower beam lengths.

C. Sailing

The sailing controller was first tested in controlled conditions, by positioning the robot at different angles to the wind and measuring the resulting sail orientation. The results of this test are shown in Fig. 11. It can be observed that the experimental data replicates the simulated results (based on Eq. 3, cf. Sec. V) accurately, with only minor discrepancies until the actuators saturate at a sail angle of approximately 60°. As a next step, the controller was tested in a water tank, using fans to artificially generate wind. Fig. 12(b) shows a

cross-wind sailing manoeuvre as an example. In this test the rudder is fixed to a given angle. The robot is autonomously able to maintain its heading and move upwind effectively.

VII. Conclusions

In this paper we have presented a novel design concept for a hybrid robot capable of both aerial and water surface locomotion. The proposed robot can perform prolonged measurements at the water surface, and simultaneously exploit the advantages of flight, including rapid deployment, reaching otherwise inaccessible areas, moving between separate bodies of water, and overcoming obstacles. Furthermore, by taking advantage of environmental vectors to move on the water surface (wind) and recharge its batteries while on the water (sun), the robot has the potential of performing long-duration missions with very limited energy consumption. A first prototype of the envisaged robot, including all key components, was implemented and tested. The robot was shown to be capable of sailing and taking off from the water, while CFD results show that stable flight is also possible. The sailing controller was found to function effectively, providing an initial degree of autonomy to the vehicle. The developed robot can be useful for applications such as water sampling, which could be significantly improved by the use of a multi-purpose, robust and energy-efficient vehicle, as compared to the current multi-vehicle solutions.

Future work will focus on pushing this platform towards an entirely renewable full outdoor operation cycle. Photovoltaic cells situated on the wing would yield sufficient power to recharge the batteries during an hour of sailing, permitting the next flight or return to base. Additionally, the control framework will be extended to achieve a fully autonomous robot. The onboard electronics were designed with a high overhead enabling further development of the open-source control software. Complementing software advances, a miniature wind direction sensor is in development which will permit sailing in changing wind conditions. Finally, further research into the hull shape design will improve our transition to flight, reducing wave production and take-off distance.

VIII. Acknowledgements

This work was funded by EPSRC (award no. EP/R009953/1, EP/L016230/1 and EP/R026173/1), NERC (award no. NE/R012229/1) and the EU H2020 AeroTwin project (grant ID 810321). Mirko Kovac is supported by the Royal Society Wolfson fellowship (RSWF/R1/18003).

References

[1] X. Yang, T. Wang, J. Liang, G. Yao, and M. Liu, "Survey on the novel hybrid aquatic-aerial amphibious aircraft aquatic unmanned aerial vehicle (AquaUAV)," *Progress in Aerospace Sciences*, 2015.

[2] J.-P. Ore, S. Elbaum, A. Burgin, and C. Detweiler, "Autonomous aerial water sampling," *Journal of Field Robotics*, vol. 32, no. 8, pp. 1095–1113, 2015. [Online]. Available: https://onlinelibrary.wiley.com/doi/abs/10.1002/rob.21591

[3] R. Bogue, "Underwater robots: a review of technologies and applications," *Industrial Robots*, vol. 42, no. 3, pp. 186–191, 2015.

[4] N. A. Cruz and A. C. Matos, "The mares auv, a modular autonomous robot for environment sampling," pp. 1–6, 2008.

[5] R. K. Katzschmann, J. DelPreto, R. MacCurdy, and D. Rus, "Exploration of underwater life with an acoustically controlled soft robotic fish," *Science Robotics*, vol. 3, no. 16, 2018.

[6] I. S. Silva, F. Campopiano, G. S. V. Lopes, A. K. Uenojo, H. T. Silva, E. L. Pellini, A. A. Alvarez, and E. A. Barros, "Development of a trimaran asv," *IFAC-PapersOnLine*, vol. 51, no. 29, 2018.

[7] Saildrone project. (retrieved 18 Feb. 2018). [Online]. Available: https://www.saildrone.com/

[8] H. Alzu'bi, I. Mansour, and O. Rawashdeh, "Loon copter implementation of a hybrid unmanned aquatic-aerial quadcopter with active buoyancy control," *Journal of Field Robotics*, 2017.

[9] M. M. Maia, D. A. Mercado, and F. J. Diez, "Design and implementation of multirotor aerial-underwater vehicles with experimental results," in *2017 IEEE/RSJ International Conference on Intelligent Robots and Systems (IROS)*, 2017, pp. 961–966.

[10] R. Peloquin, D. Thibault, and A. L. Desbiens, "Design of a passive vertical takeoff and landing aquatic UAV," *IEEE Robotics and Automation Letters*, vol. 2, no. 2, pp. 381–388, April 2017.

[11] J. Liang, Y. Xing, W. Tianmiao, Y. Guocai, and W. Zhao, "Design and experiment of a bionic gannet for plunge-diving," *Journal of Bionic Engineering*, vol. 10, no. 3, 2013.

[12] J. Moore, A. Fein, and W. Setzler, "Design and analysis of a fixed-wing unmanned aerial-aquatic vehicle," in *2018 IEEE International Conference on Robotics and Automation (ICRA)*, 2017.

[13] R. Siddall and M. Kovač, "Launching the AquaMAV: Bioinspired design for aerial-aquatic robotic platforms," *Bioinspiration and Biomimetics*, vol. 9, no. 3, 2014.

[14] R. Siddall and M. Kovac, "Fast Aquatic Escape with a Jet Thruster," *IEEE/ASME Transactions on Mechatronics*, vol. 22, no. 1, pp. 217–226, 2017.

[15] Y. H. Tan, R. Siddall, and M. Kovac, "Efficient aerial-aquatic locomotion with a single propulsion system," *IEEE Robotics & Automation Letters*, vol. 2, no. 3, 2017.

[16] K. H. Low, T. Hu, S. Mohammed, J. Tangorra, and M. Kovac, "Perspectives on biologically inspired hybrid and multi-modal locomotion," *Bioinspiration Biomimetics*, vol. 10, no. 2, 2015.

[17] I. Dathe and M. de Leo, "Hydrodynamic characteristics of seaplanes as affected by hull shape parameters," *Advanced Marine vehicles conference*, 1989.

[18] S. Gudmundsson, *General Aviation Aircraft Design: Applied Methods and Procedures - Appendix C3 Design of Seaplanes*. Elsevier, September 2013.

[19] E. P. Clement and J. D. Pope, "Stepless and stepped planing hullsgraphs for performance prediction and design," *International Shipbuilding Progress*, vol. 8, no. 84, pp. 344–360, 1961.

[20] D. Savitsky, "Hydrodynamic design of planing hulls," *Marine technology*, vol. 1, no. 1, 1964.

[21] px4 autopilot. (retrieved 24 Feb. 2019). [Online]. Available: https://px4.io

[22] L. Jaulin and F. Le Bars, "A simple controller for line following of sailboats," *Robotic Sailing*, 2012.

[23] C. Viel, U. Vautier, J. Wan, and L. Jaulin, "Position keeping control of an autonomous sailboat," *IFAC Proceedings Volumes*, vol. 51, 2018.